JOURNAL OF COMPUTATIONAL PHYSICS **143,** 241–258 (1998)
ARTICLE NO. CP985964

Finite-Element Solution of Nonlinear Time-Dependent Exterior Wave Problems

Dan Givoli* and Igor Patlashenko†

**Department of Aerospace Engineering, and †Asher Space Research Center, Technion—Israel Institute of Technology, Haifa 32000, Israel*

Received April 1, 1997; revised January 13, 1998

A finite element scheme is devised for the solution of nonlinear time-dependent exterior wave problems. The two-dimensional nonlinear scalar (Klein–Gordon) wave equation is taken as a model to illustrate the method. The governing equation is first discretized in time, leading to a time-stepping scheme, where a nonlinear exterior elliptic problem has to be solved in each time step. An artificial boundary $\mathcal{B}$ is introduced, which bounds the computational domain Ω, and a simple-iteration procedure is used to linearize the problem in the infinite domain outside $\mathcal{B}$. This enables the derivation of a Dirichlet-to-Neumann boundary condition on $\mathcal{B}$. Finite element discretization and Newton iteration are finally employed to solve the problem in Ω. The computational aspects of this method are discussed. Numerical results are presented for the nonlinear wave equation, whose solutions may blow up in a finite time under certain conditions, and it is shown that the behavior of the solution predicted by theory is captured by the scheme.

Key Words: nonlinear waves; Dirichlet-to-Neumann (DtN); finite element; exterior problems.

1. INTRODUCTION

Nonlinear waves in unbounded media are encountered in a variety of applications [1–3]. The nonlinearity may originate from the material constitutive relations, from the large amplitude of the motion, or from the presence of a free boundary. In most cases, the nonlinear governing equations are time-dependent; pure time-harmonic waves are not possible in the nonlinear regime. For this and other reasons, the theoretical and computational analysis of nonlinear wave problems is typically complicated. The computational treatment of the unboundedness of the problem domain is an additional difficulty which must be dealt with.

Most numerical methods for unbounded domain problems [4] are not directly designed to account for nonlinearities in the exterior domain. In fact, some methods, like

0021-9991/98 $25.00

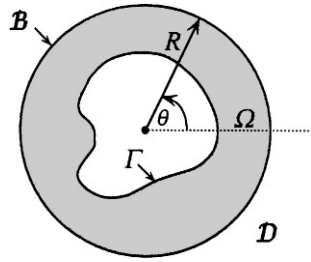

FIG. 1. A typical setup of the DtN method for exterior problems.

boundary-element schemes [5]. Dirichlet-to-Neumann (DtN) finite-element schemes [6], and some infinite-element schemes [7], are based on an exact solution of the governing equations in the far field, and such an exact solution is not available with nonlinearities which extend to infinity.

In this paper we devise a new DtN-type numerical method for nonlinear exterior wave problems. The DtN finite element method was originally developed for the solution of linear elliptic problems in infinite domains [6, 8–10] and can be summarized as follows. First, a simple-shaped artificial boundary $\mathcal{B}$ is introduced, which divides the original infinite domain into two domains: a finite computational domain Ω and an infinite residual domain D (see Fig. 1). Then, by analyzing the problem in D, an exact relation on $\mathcal{B}$, which is based on the associated Dirichlet-to-Neumann map, is derived. This relation is used as a boundary condition on $\mathcal{B}$ (called the DtN boundary condition) to obtain a new well-posed problem in Ω. This new problem is equivalent to the original infinite-domain problem in that both problems have the same solution in Ω. Finally, the new problem in Ω is solved by the finite-element method.

In the context of linear wave problems, the DtN condition on $\mathcal{B}$ is a perfectly nonreflecting boundary condition [11]. Analysis and some improvements of the DtN method can be found in [12–17]. Closely related schemes for various problems and configurations were devised in [18–22]. Other types of schemes that involve exact treatment of the far field have also been used [23–25].

In [26], the DtN method was extended to treat the time-dependent (hyperbolic) wave equation, still in the linear regime. Recently, several DtN-type schemes have been proposed for a class of nonlinear elliptic problems [27], of the form $\nabla^2 u + f(u) = 0$ (cf. also [23]). Here, we combine some of the ideas of [26] and [27] to obtain a new scheme for nonlinear time-dependent wave problems. We do this in the context of a model problem, governed by the two-dimensional nonlinear scalar (Klein–Gordon) equation [28]. This equation has important applications in quantum physics. It also describes waves in a membrane lying on a nonlinear elastic foundation. However, more importantly, it serves as a relatively simple model for nonlinear wave problems which helps to bring to light some theoretical issues and typical computational difficulties.

Following is the outline of the paper. In Section 2 we state the model problem under consideration. In Section 3 we discretize the nonlinear wave equation in time, using the two-parameter implicit Newmark family of time integration schemes. This leads to a time-stepping scheme, where a nonlinear exterior elliptic problem has to be solved in each time step. In Section 4 we introduce an artificial boundary $\mathcal{B}$ which bounds the computational domain Ω. Then we apply a simple-iteration procedure to repeatedly linearize the elliptic

problem in the infinite domain D outside $\mathcal{B}$. Once a linear elliptic problem is defined in D, it is possible to derive an exact DtN boundary condition on $\mathcal{B}$; this is done in Section 5. In Section 6 we discuss the finite-element formulation in Ω. The whole solution procedure is summarized and commented on in Section 7. In Section 8 we present some numerical results, check their accuracy, and compare their global behavior to that predicted by theory [28]. We conclude with some remarks in Section 9.

2. STATEMENT OF THE PROBLEM

We consider the two-dimensional infinite domain $\mathcal{R}$ outside an obstacle with boundary Γ. In $\mathcal{R}$, the nonlinear version of the Klein–Gordon equation governs [28]:

$$\ddot{u} - c^2\nabla^2 u = f(u). \tag{1}$$

Here $u(x, t)$ is the unknown wave function, x is the position vector in space, t is time, c is a given constant wave speed, and $f(u)$ is a given nonlinear function. A superposed dot denotes differentiation with respect to t. We note in passing that when $f(u) = -\omega_0^2 u$, (1) becomes the linear Klein–Gordon equation.

The obstacle boundary Γ is divided into two parts: $\Gamma = \Gamma_g \cup \Gamma_h$. On Γ_g, a Dirichlet condition is given, whereas on Γ_h, a Neumann condition is given:

$$u = g \qquad \text{on } \Gamma_g \tag{2}$$

$$\frac{\partial u}{\partial \nu} = h \qquad \text{on } \Gamma_h. \tag{3}$$

Here $\partial/\partial\nu$ is the normal derivative on Γ_h, and g and h are given functions. Initial conditions are given for u and $\dot{u}$:

$$u(x, 0) = u_0(x), \qquad \dot{u}(x, 0) = v_0(x). \tag{4}$$

Here u_0 and v_0 are given functions with compact support. At infinity the solution is bounded. Since the differential operator in (1) is hyperbolic, there is no need in a "radiation condition" at infinity to complete the statement of the problem, even though the solution can be shown to satisfy such a condition [29].

3. TIME DISCRETIZATION

The first step in the proposed numerical method is to *discretize the problem in time*. To fix ideas we choose the Newmark family of time-integration schemes, although other algorithms can be considered as well. Let Δt be the (constant) time-step interval, and let t_n be the time after n time steps. Also, let u_n, v_n, and a_n be the approximations of u, $\dot{u}$, and $\ddot{u}$ at time t_n. The Newmark method applied to Eq. (1) consists of the three equations

$$a_{n+1} - c^2\nabla^2 u_{n+1} = f(u_{n+1}) \tag{5}$$

$$u_{n+1} = u_n + \Delta t v_n + \frac{(\Delta t)^2}{2}[(1 - 2\beta)a_n + 2\beta a_{n+1}] \tag{6}$$

$$v_{n+1} = v_n + \Delta t[(1 - \gamma)a_n + \gamma a_{n+1}]. \tag{7}$$

Here $0 < \beta \leq 0.5$ and $0 \leq \gamma \leq 1$ are two parameters which determine the stability and accuracy properties of the scheme. We are interested only in *implicit* schemes, and therefore we exclude the case $\beta = 0$.

After some algebra, Eqs. (5)–(7) yield the recursive formulae

$$(1-(\Delta t)^2\beta c^2\nabla^2)u_{n+1} = u_n + \Delta t v_n + \frac{(\Delta t)^2}{2}[(1-2\beta)a_n + 2\beta f(u_{n+1})] \tag{8}$$

$$a_{n+1} = \frac{1}{2\beta}\left[\frac{2}{(\Delta t)^2}(u_{n+1}-u_n-\Delta t v_n) - (1-2\beta)a_n\right] \tag{9}$$

$$v_{n+1} = v_n + \Delta t[(1-\gamma)a_n + \gamma a_{n+1}]. \tag{10}$$

Note that (8) is an elliptic partial differential equation for u_{n+1}. The time-discrete version of the boundary conditions (2) and (3) as well as the boundedness condition at infinity must be added to (8) to complete the statement of the problem. From an implementational viewpoint it is beneficial to write these equations in a predictor–corrector form, namely:

Prediction:

$$\tilde{u}_{n+1} = u_n + \Delta t v_n + \frac{(\Delta t)^2}{2}(1-2\beta)a_n \tag{11}$$

$$\tilde{v}_{n+1} = v_n + \Delta t(1-\gamma)a_n. \tag{12}$$

Solution:

$$(1-(\Delta t)^2\beta c^2\nabla^2)u_{n+1} = \tilde{u}_{n+1} + (\Delta t)^2\beta f(u_{n+1}) \tag{13}$$

$$u_{n+1} = g_{n+1} \qquad \text{on } \Gamma_g \tag{14}$$

$$\frac{\partial u_{n+1}}{\partial \nu} = h_{n+1} \qquad \text{on } \Gamma_h \tag{15}$$

$$u_{n+1} < \infty \qquad \text{at infinity.} \tag{16}$$

Correction:

$$a_{n+1} = \frac{1}{\beta(\Delta t)^2}(u_{n+1}-\tilde{u}_{n+1}) \tag{17}$$

$$v_{n+1} = \tilde{v}_{n+1} + \gamma\Delta t a_{n+1}. \tag{18}$$

Thus, in addition to the updating performed in the prediction and correction phases, one has to solve in each time step the elliptic problem (13)–(16) in the unbounded domain $\mathcal{R}$.

To write (13) more concisely we define

$$\alpha = \left(c\Delta t\sqrt{\beta}\right)^{-1}, \qquad \tilde{f}(u_{n+1}) = -\tilde{u}_{n+1} - (\Delta t)^2\beta f(u_{n+1}). \tag{19}$$

Then (13) becomes

$$\alpha^{-2}\nabla^2 u_{n+1} - u_{n+1} = \tilde{f}(u_{n+1}). \tag{20}$$

4. LINEARIZATION VIA SIMPLE ITERATION

We now introduce a circular artificial boundary $\mathcal{B}$ of radius R which encloses the obstacle and bounds the computational domain Ω. The infinite domain outside $\mathcal{B}$ is denoted D, i.e., $D = \mathcal{R} - \Omega$ (see Fig. 1).

We employ a simple-iteration procedure to replace the nonlinear equation (20) in D by a sequence of linear equations. The solution u_{n+1} in iteration i is denoted $u_{n+1}^{(i)}$. Equation (20) is replaced by

$$\alpha^{-2}\nabla^2 u_{n+1}^{(i+1)} - u_{n+1}^{(i+1)} = \tilde{f}\left(u_{n+1}^{(i)}\right) \qquad \text{in } D. \tag{21}$$

Since $u_{n+1}^{(i)}$ is known at the $i+1$ iteration, the function $\tilde{f}$ in (21) is just a given function of x, and thus (21) is a *linear* elliptic equation. Also, the boundedness condition (16) is written as

$$u_{n+1}^{(i+1)} < \infty \qquad \text{at infinity} \tag{22}$$

Note that (21) replaces (20) only in the exterior domain D. In the computational domain Ω, the governing equation remains the nonlinear equation (20).

5. DtN BOUNDARY CONDITION

Now we shall derive an exact boundary condition on $\mathcal{B}$ for $u_{n+1}^{(i+1)}$. This condition is derived by finding a solution in D, which exactly satisfies Eqs. (21) and (22), as well as the obvious condition

$$u_{n+1}^{(i+1)} = u_{n+1}^{(i+1)}(R,\theta) \qquad \text{on } \mathcal{B}. \tag{23}$$

In the remainder of this section we shall omit the indices $n+1$ and $(i+1)$ for brevity. We shall also use $\tilde{f}$ to mean $\tilde{f}(u_{n+1}^{(i)})$. Note that at the current iteration $\tilde{f}$ is a known function.

The problem (21)–(23) is solved by the method of variation of parameters. We seek a solution of the form

$$u(r,\theta) = {\sum_{m=0}^{\infty}}' [C_m(r)\cos m\theta + D_m(r)\sin m\theta]. \tag{24}$$

The prime after the sum indicates that the term $m=0$ is multiplied by a factor of $1/2$. We substitute (24) into (21) and for each m we equate the coefficients of $\cos m\theta$ and $\sin m\theta$. This results in the following uncoupled set of ordinary differential equations for $m = 0, 1, 2, \ldots$:

$$\alpha^{-2}\left(C_m'' + \frac{1}{r}C_m' - \frac{m^2}{r^2}C_m\right) - C_m = \tilde{f}_m^c(r) \tag{25}$$

$$\alpha^{-2}\left(D_m'' + \frac{1}{r}D_m' - \frac{m^2}{r^2}D_m\right) - D_m = \tilde{f}_m^s(r). \tag{26}$$

Here a prime denotes differentiation with respect to r. The functions $\tilde{f}_m^c(r)$ and $\tilde{f}_m^s(r)$ are respectively the cosine and sine coefficients in the Fourier decomposition of the function $\tilde{f}$. Also, substituting (24) into the boundary condition (23) results in

$$C_m(R) = \frac{1}{\pi}\int_0^{2\pi} \cos m\theta\, u(R,\theta)\, d\theta \tag{27}$$

$$D_m(R) = \frac{1}{\pi}\int_0^{2\pi} \sin m\theta\, u(R,\theta)\, d\theta. \tag{28}$$

Equations (25)–(28) can be written in the general form

$$r^2y'' + ry' - (\alpha^2 r^2 + m^2)y = \hat{f}(r) \tag{29}$$

$$y(R) = Y_R. \tag{30}$$

The general solution of the *homogeneous* counterpart of (29) is $AI_m(\alpha r) + BK_m(\alpha r)$, where I_m and K_m are the modified Bessel functions of the first and second kind. To satisfy (22), the homogeneous solution must involve only K_m and not I_m. Imposing (30) in addition yields the solution

$$y_{\text{hom}}(r) = Y_R \frac{K_m(\alpha r)}{K_m(\alpha R)}. \tag{31}$$

Since (31) satisfies the homogeneous counterpart of (29) and the condition (30), we now seek a particular solution which satisfies (29) and the homogeneous counterpart of (30). This particular solution is obtained by deriving first the associated Green's function. The Green's function is found to be [29]

$$\xi^2 G_m(r,\xi) = \begin{cases} \phi_m(\xi)\psi_m(r)[E_m(\xi)]^{-1}; & r \le \xi \\ \psi_m(\xi)\phi_m(r)[E_m(\xi)]^{-1}; & r \ge \xi \end{cases}, \tag{32}$$

where

$$\phi_m(\xi) = K_m(\alpha\xi) \tag{33}$$

$$\psi_m(\xi) = I_m(\alpha\xi)K_m(\alpha R) - K_m(\alpha\xi)I_m(\alpha R) \tag{34}$$

$$E_m(\xi) = \psi_m(\xi)\phi_m'(\xi) - \phi_m(\xi)\psi_m'(\xi). \tag{35}$$

Using this Green's function, the particular solution is

$$y_{\text{p}}(r) = \int_R^\infty G_m(r,\xi)\,\hat{f}(\xi)\,d\xi. \tag{36}$$

The solution of (29) and (30) is the sum of y_{hom} in (31) and y_{p} in (36). We are now able to write the solution of (25)–(28) for the coefficients $C_m(r)$ and $D_m(r)$. These expressions are substituted in the Fourier series (24) and after some algebra we get the solution $u(r,\theta)$ in the domain D. The end result is

$$u(r,\theta) = \frac{1}{\pi}{\sum_{m=0}^{\infty}}' \frac{K_m(\alpha r)}{K_m(\alpha R)} \int_0^{2\pi} \cos m(\theta-\theta')u(R,\theta')\,d\theta'$$

$$+\alpha^2 {\sum_{m=0}^{\infty}}' \int_R^\infty \xi^2 G_m(r,\xi)\left(\tilde{f}_m^c(\xi)\cos m\theta + \tilde{f}_m^s(\xi)\sin m\theta\right)d\xi. \tag{37}$$

We now differentiate both sides of (37) with respect to r and then set $r = R$. After some algebra, and using the properties of the modified Bessel functions, we get

$$\frac{\partial u}{\partial r} = -Mu + H[\tilde{f}] \qquad \text{on } \mathcal{B} \tag{38}$$

$$Mu = {\sum_{m=0}^{\infty}}' \int_0^{2\pi} k_m(\theta-\theta')\,u(R,\theta')\,d\theta' \tag{39}$$

$$k_m(\theta-\theta') = -\frac{\alpha}{\pi}\frac{K_m'(\alpha R)}{K_m(\alpha R)}\cos m(\theta-\theta') \tag{40}$$

$$H[\tilde f](\theta) = \alpha^2 {\sum_{m=0}^{\infty}}' \int_R^\infty B_m(\xi)\left[\tilde f_m^c(\xi)\cos m\theta + \tilde f_m^s(\xi)\sin m\theta\right] d\xi \tag{41}$$

$$B_m(\xi) = -\frac{K_m(\alpha\xi)}{K_m(\alpha R)}\frac{\xi}{R} \tag{42}$$

$$\tilde f_m^c(\xi) = \frac{1}{\pi}\int_0^{2\pi}\cos m\theta\,\tilde f(\xi,\theta)\,d\theta, \qquad \tilde f_m^s(\xi) = \frac{1}{\pi}\int_0^{2\pi}\sin m\theta\,\tilde f(\xi,\theta)\,d\theta. \tag{43}$$

Equation (38) is an exact Dirichlet-to-Neumann boundary condition on $\mathcal{B}$, similar to the one obtained in [26] in the linear case. It is exact with respect to Eqs. (21)–(23), although, of course, it is not exact with respect to the original time-dependent nonlinear problem. Two approximations which must be made in practice are the truncation of the sums in (39) and (41) after a finite number of terms, and the numerical integration needed in (41); see Section 7. The integral in (39) can be evaluated exactly, as is done in [6, 26].

If we now recover the indices $n+1$ and $(i+1)$, the DtN boundary condition (38) becomes

$$\frac{\partial u_{n+1}^{(i+1)}}{\partial r} = -Mu_{n+1}^{(i+1)} + H\left[\tilde f\left(u_{n+1}^{(i)}\right)\right] \qquad \text{on } \mathcal{B}. \tag{44}$$

Note that H in (44) is a known function at the $(i+1)$ iteration.

6. FINITE-ELEMENT FORMULATION

At time step $n+1$ and at simple-iteration $(i+1)$, the problem to be solved in Ω consists of the nonlinear elliptic equation (20), the boundary conditions (14) and (15) on Γ, and the DtN boundary condition (44) on $\mathcal{B}$. This problem is solved by the Galerkin finite-element method. The weak form of the problem is formally similar to that given in [26] in the linear case. Finite-element discretization leads to the system of nonlinear algebraic equations

$$Kd_{n+1} = F_{n+1}(d_{n+1}), \tag{45}$$

where

$$K = K^a + K^b, \qquad F_{n+1} = F_{n+1}^a + F_{n+1}^b \tag{46}$$

$$K_{AB}^a = a(N_A, N_B) \tag{47}$$

$$K_{AB}^b = b(N_A, N_B) \tag{48}$$

$$\left(F_{n+1}^a\right)_A = (N_A,\ \tilde f(u_{n+1})) - \sum_{B\in\eta_g}(g_{n+1})_B\, a(N_A, N_B) \tag{49}$$

$$\left(F_{n+1}^b\right)_A = \left(N_A, H\left[\tilde f\left(u_{n+1}^{(i)}\right)\right]\right)_{\mathcal{B}}. \tag{50}$$

Here the following bilinear forms are used:

$$a(w,u) = \alpha^{-2}\int_\Omega \nabla w\cdot\nabla u\,d\Omega + \int_\Omega wu\,d\Omega \tag{51}$$

$$b(w,u) = \alpha^{-2}\int_B wMu\,d\mathcal{B} \tag{52}$$

$$(w, f) = \int_\Omega wf \, d\Omega \tag{53}$$

$$(w, H)_{\mathcal{B}} = \alpha^{-2} \int_B wH \, d\mathcal{B}. \tag{54}$$

In (47)–(50), A and B are indices corresponding to global node numbers A and B, and N_A is the finite element shape function associated with node A. In (49), η_g is the set of all nodes on Γ_g, and $(g_{n+1})_B$ is the value of the function g_{n+1} at node B on Γ_g. In (45), K is the global stiffness matrix, d is the solution vector, and F is the load vector. We omit the index $(i+1)$ from all the variables in (45)–(50) for brevity; however, in (50) we indicate that H is calculated based on u from the previous iteration, i.e., $u_{n+1}^{(i)}$. The nonlinearity of (45) is due to the dependence of the load vector F on the solution vector d, through $\tilde{f}(u_{n+1})$ in (49).

The nonlinear algebraic system (45) is solved using Newton iterations. At Newton iteration $j+1$, the solution is updated via

$$d^{j+1} = d^j + \Delta d^j, \tag{55}$$

where the incremental vector Δd^j is found by solving the linear system of equations

$$K_t^j \Delta d^j = R^j. \tag{56}$$

Here K_t^j is the tangent stiffness matrix, and R^j is the residual vector. They are given by

$$K_t^j = K - \frac{\partial F^a}{\partial d}(d^j) \tag{57}$$

$$R^j = F(d^j) - Kd^j. \tag{58}$$

The last term on the right side of (57) can be expressed explicitly by

$$\left[\frac{\partial F^a}{\partial d}(d^j)\right]_{AB} \equiv \frac{\partial F_A^a}{\partial d_B}(d^j) = \int_\Omega N_A \tilde{f}' \left(\sum_C N_C d_C^j\right) N_B \, d\Omega. \tag{59}$$

Thus, the tangent stiffness matrix K_t^j is symmetric.

7. SOLUTION PROCEDURE

The entire solution procedure is summarized in Box 1. We now make some comments on the computational aspects of this procedure.

Remark 1. This solution scheme consists of *three loops*: the time-step loop (indicated by n), the simple-iteration loop (indicated by i), and the Newton-iteration process which is the innermost loop (indicated by j). The convergence criterion for stopping either of the latter two processes is based on evaluating the residual norms and comparing them to some given tolerances.

Remark 2. The matrix $K = K^a + K^b$ in (45), (46) remains constant during the time stepping; only the right-hand side F_{n+1} is changing. Thus, K has to be formed and factorized only once, outside of the time-step loop. This also implies that the effort it requires is marginal for an analysis with many time steps.

Remark 3. The computation of $H[\tilde{f}]$ in (41) involves the computation of the Fourier coefficients of the function $\tilde{f}$ given by (19), for $\xi \geq R$. Thus, it is necessary to keep track

BOX 1

General Solution Procedure for the Time-Dependent Nonlinear Exterior Wave Problem

* Time-step loop: $n = 0, 1, 2, \ldots$
- **1.** Compute the predicted values $\tilde{u}_{n+1}$ and $\tilde{v}_{n+1}$ in Ω by using (11), (12).
- **2.** Compute the predicted values $\tilde{u}_{n+1}$ and $\tilde{v}_{n+1}$ at integration points in D by using (11), (12).
- **3.** $u_{n+1}^{(0)} \equiv \tilde{u}_{n+1}$.
- * Simple-iteration loop: $i = 0, 1, 2, \ldots$
  - **4.** Use (41) to find $H[\tilde{f}(u_{n+1}^{(i)})]$ on $\mathcal{B}$.
  - * Newton-iteration loop: $j = 0, 1, 2, \ldots$
    - **5.** Perform a single Newton iteration: solve (56) and use (55) to update the solution in Ω.
    - **6.** Check convergence. If converged, $u_{n+1}^{(i+1)}$ in Ω is obtained; go to step 7.
  - * Next j
  - **7.** Use (37), with $\tilde{f} = \tilde{f}(u_{n+1}^{(i)})$, to find $u_{n+1}^{(i+1)}$ at integration points in D.
  - **8.** Check convergence. If converged, u_{n+1} is obtained; go to step 9.
- * Next i
- **9.** Correct a_{n+1} and v_{n+1} in Ω by using (17), (18).
- **10.** Correct a_{n+1} and v_{n+1} at integration points in D by using (17), (18).

* Next time step

of $\tilde{u}_{n+1}$, defined by (11), in D. To this end, and for the purpose of performing the integration in (41) and (37), the annular domain $R \leq r \leq r_{\max}$ is divided into integration cells with polar geometry. This has been done in [26] in the linear case and is also often done in the boundary-element method to evaluate infinite-domain integrals. The integrals in (41) and (37) are calculated numerically by using a simple trapezoidal rule per integration cell in both the r- and θ-directions. The use of a Laguerre integration rule in D (see [30]) as an alternative to this procedure has been checked and found not as effective for the time-dependent case. A discussion on the accuracy of the exterior integration, as well as example error calculations, is presented in [30] for the linear elliptic case, when there is an inhomogeneity (i.e., sources) in the exterior.

In choosing the truncation distance $r_{\max}$, one can exploit the fact that the fastest wave fronts advance with velocity c. This is true regardless of the dispersive and nonlinear nature of the waves. This fact can be proved easily by considering the standard integral representation of the solution using the Riemann kernel for the linear wave equation with u-dependent forcing. Such a consideration shows that with the nonlinear equation (1), where $f(0) = 0$, if the solution exists globally then no group velocity can be larger than the characteristic velocity c. In other words, c is the largest possible speed of the propagating waves. This property is also exhibited in the numerical experiments (see Section 8).

In this light, the truncation distance $r_{\max}$ need not be constant during the time stepping. In fact, $r_{\max}$ may be chosen at each time step such that it is always just ahead of the wave fronts which advance with velocity c. Moreover, there is no point in increasing $r_{\max}$ beyond a certain distance where the amplitude of the waves is believed to be sufficiently small so as not to affect the value of the integrals in (41) and (37).

Once the size of the exterior integration region (i.e., the distance $r_{\max}$) is determined, the size and number of the integration cells may be chosen so as to have a sufficient number of

cells per wavelength, to the accuracy and scale that is desired. Since the same considerations also determine the density of the finite element mesh inside Ω, having the size of the cells equal to the size of the elements in Ω adjacent to $\mathcal{B}$ is a reasonable choice.

It may appear that we are computing in a large domain (which is to be avoided due to computational inefficiency); however, it should be noted that only an *integration* is performed here over a large domain, and not the solution of a partial differential equation.

Remark 4. The expressions for M and $H[\tilde{f}]$ (see (39) and (41)) involve infinite series. In practice all the infinite sums are truncated after a finite number of terms, N. The associated truncation error and convergence properties (for linear problems), including the rate of convergence with N, were estimated and measured recently in [17]. Generally, only a few terms are needed to achieve a satisfactory level of accuracy.

Remark 5. The computationally intensive part of the algorithm is the evaluation of the infinite integrals appearing in (41) and (37), as discussed in Remark 3 above. In [27] we considered a special simplified procedure, albeit for time-independent problems, that significantly reduces the computational effort involved. The quadratic asymptotic boundary condition proposed by Hagstrom [23] also deals with similar difficulties for a class of nonlinear problems in cylinders. However, we have found that in the time-dependent case, the accuracy achieved by the simplified scheme deteriorates rapidly in time, and therefore we use the full scheme based on simple iteration in this case.

8. NUMERICAL EXAMPLES

Now we present a few numerical results for problems governed by the nonlinear wave equation (1). Strauss [28] has shown that solutions to (1) either exist globally or blow up in a finite time, depending on the nonlinear function $f(u)$ and sometimes also on the initial data. For example, it can be proved that if $f(u) = -u^3$, then all solutions exist globally (for $t < \infty$), while if $f(u) = u^2$ or $-u^2$, then all solutions blow up in a finite time. These theorems are proved in [28] for the three-dimensional case, but our numerical results show that the same behavior is obtained in two dimensions.

To measure the accuracy of our numerical results, we construct a reference solution which we refer to in what follows as the "exact" solution. This solution is obtained by performing the calculation with a relatively large computational domain Ω, a very fine mesh, and a large integration exterior domain with many integration cells (all relative to the actual numerical solution under consideration). We also make the convergence tolerances extremely small. On the other hand, the time-step size used, Δt, is the same as in the actual computational model; i.e., we do not attempt to make the temporal error smaller than that which the time integration scheme produces. We denote the reference solution obtained in this manner by u_{ex}.

We first consider an axisymmetric problem, with $c = 200$ and $f(u) = -qu^3$, where q is a positive constant. The obstacle is a circle of radius $a = 0.25$. The initial values of u and $\dot{u}$ (see (4)) are zero throughout the infinite domain. On the obstacle boundary Γ we prescribe $u = 1$ at time $t \geq 0$. Thus, the obstacle is at rest at $t = 0^-$ and starts to radiate cylindrical waves at $t = 0^+$.

Figures 2a–2d show the "exact" solution, u_{ex}, as a function of the radial coordinate r, for four times ($t = 0.01, 0.1, 0.2$, and 0.3) and three values of the nonlinearity parameter q ($q = 0, 10^4$, and 2×10^5). At very small times, the nonlinearity does not have a strong

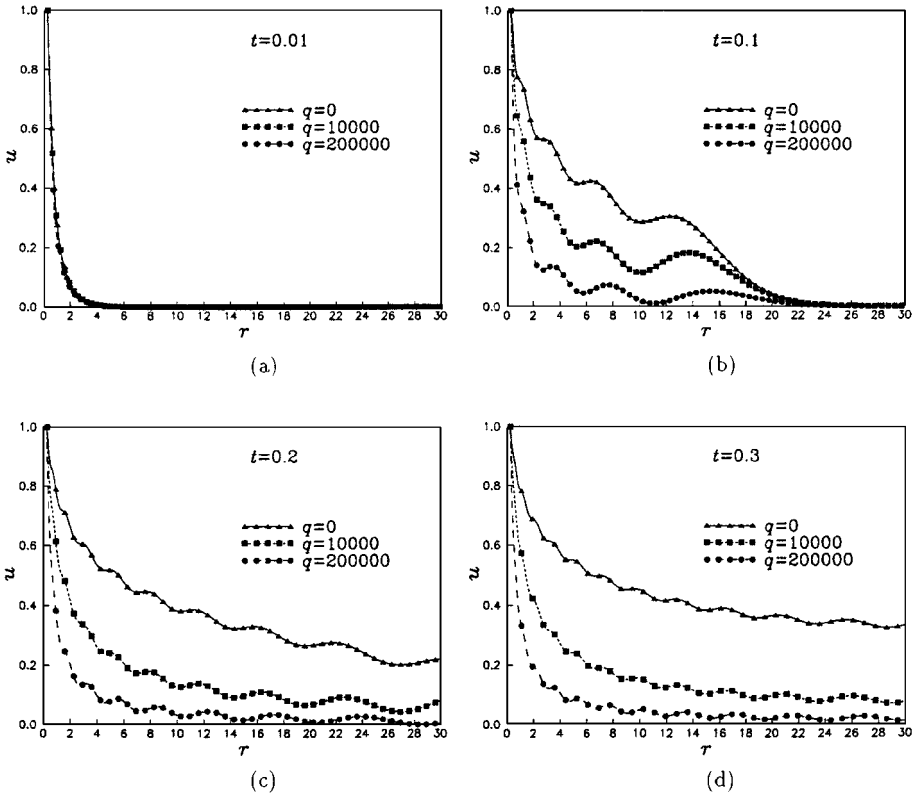

FIG. 2. An axisymmetric example, $f(u) = -qu^3$. "Exact" solutions as functions of the radial coordinate r for three values of the nonlinearity parameter q (a) at $t = 0.01$, (b) at $t = 0.1$, (c) at $t = 0.2$, and (d) at $t = 0.3$.

effect on the solution, and the three solutions in Fig. 2a almost coincide. For larger times, the nonlinearity becomes very significant. The solution to the linear problem ($q = 0$) has the largest magnitude at a given radial location, but all waves propagate with the same speed; in Fig. 2b the wave front reaches $r = ct = 20$ for all three solutions. This is expected: see Remark 3 in Section 7.

The computational parameters are as follows. We set the circular artificial boundary at $R = 0.5$. The finite element mesh consists of 3 layers of bilinear quadrilateral elements, with 24 elements in each layer. We use the Newmark time integration scheme (see Section 3) with parameters $\beta = 0.25$ and $\gamma = 0.5$. This is the unconditionally stable implicit second-order average acceleration scheme. We use a time step of $\Delta t = 0.01$, which amounts to a Courant number of about 24. This means that the fastest waves propagate at a rate of about 24 elements per time step (although, due to the dispersive nature of the solution, there are slower waves, too). Of course, this is possible only with an unconditionally stable scheme and may lead to insufficient temporal accuracy. The accuracy can be improved by taking a smaller time step or a higher-order time integration scheme.

For the integration in the exterior domain (see Section 7, Remark 3) we use $r_{\max} = 50, 250$ integration cells in the radial direction, and 24 cells in the circumferential direction. We use $N = 10$ terms in the DtN expansion. The residual-norm tolerances used for terminating the simple-iteration and Newton-iteration processes (see Box 1 and Section 7, Remark 1) are both 10^{-5}.

TABLE 1
An Axisymmetric Example, $f(u) = -qu^3$: "Exact" Solution and Error at Various Times for Three Values of q

	$q = 0$		$q = 10{,}000$		$q = 200{,}000$	
t	"Exact"	Error	"Exact"	Error	"Exact"	Error
0.01	0.6022	0.0004	0.5978	0.0004	0.5381	0.0002
0.02	0.9441	0.0014	0.9164	0.0009	0.7089	0.0001
0.03	0.7528	0.0002	0.7059	0.0001	0.4979	0.0006
0.04	0.9081	0.0022	0.8536	0.0018	0.6861	0.0005
0.05	0.8174	0.0003	0.7509	0.0004	0.5534	0.0011
0.06	0.8825	0.0030	0.8119	0.0020	0.6378	0.0006
0.07	0.8558	0.0016	0.7796	0.0002	0.5960	0.0011
0.08	0.8673	0.0031	0.7867	0.0014	0.6080	0.0005
0.09	0.8790	0.0036	0.7965	0.0012	0.6167	0.0004
0.1	0.8598	0.0033	0.7736	0.0005	0.5960	0.0002

In Table 1 some numerical results are given for this example, at various times and for the three values of q mentioned before. The value of the "exact" solution u_{ex}, as well as the error defined by $|u^h - u_{ex}|$ (where u^h is the finite element solution), is given at $r = R$. The errors are very small in all cases relative to the solution itself. It is interesting to note that at most time steps (although not for all of them) the error is smaller for the larger values of q; the strongly nonlinear case leads to more accurate results. Moreover, the error increases with time in the linear case and maintains the same level in the nonlinear cases. These observations are related to the behavior of the solutions observed in Fig. 2; the solution to the linear problem ($q = 0$) "decays" less rapidly as r increases, and thus its numerical integration in the exterior domain is more demanding. Similar behavior is observed for later times.

Now we turn to the case $f(u) = qu^2$, where q is a positive constant. All the other parameters are the same as in the previous example. Figures 3a–3c show the solutions at $r = R$ obtained as functions of time for three values of q ($q = 0$, 2000, and 5000). Three solutions are shown for each value of q: the "exact" solution, the solution obtained by the procedure proposed in this paper and using the DtN boundary condition on $\mathcal{B}$, and the solution obtained by using a Sommerfeld-like local boundary condition on $\mathcal{B}$ [4, 11]. In the latter case the nonlinear problem is solved in Ω, but the exterior domain D is disregarded altogether. In the linear case ($q = 0$), as shown in Fig. 3a, the DtN solution agrees very well with the "exact" solution, whereas the Sommerfeld condition produces a large error. This is expected, since it is well known that the Sommerfeld-like boundary condition generates large spurious reflections from $\mathcal{B}$ [11].

The agreement between the DtN and "exact" solutions is also apparent in the nonlinear cases, shown is Figs. 3b and 3c. The difference between these solutions and the Sommerfeld solution is even more dramatic here. Whereas the "exact" and DtN solutions "blow up" in a finite time (as they should according to the theory [28]; see discussion above), the Sommerfeld solution remains bounded and oscillatory about $u = 1$! (In fact, the Sommerfeld solution changes only slightly when q is changed.) It is also interesting to note that the "blow up" occurs at an earlier time for a larger value of the nonlinearity parameter q.

Next, we return to the case $f(u) = -qu^3$, for which the solution exists globally, and we set $q = 2 \times 10^5$. On the obstacle surface Γ we prescribe $u = 1 + \cos 2\theta$. All

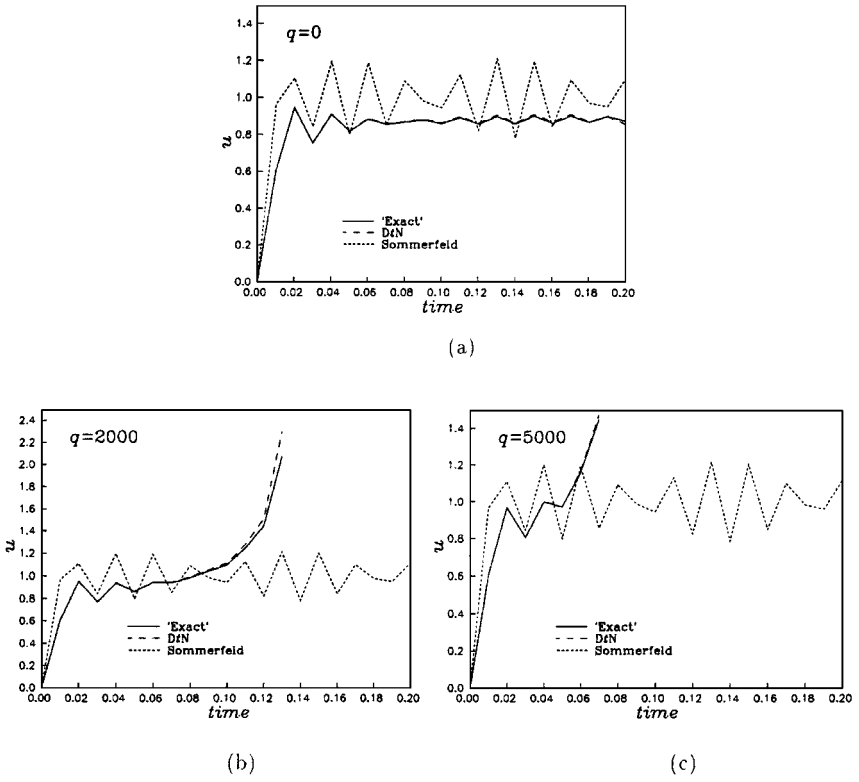

FIG. 3. An axisymmetric example, $f(u) = qu^2$. Comparison of solutions at $r = R$ as a function of time at (a) $q = 0$, (b) $q = 2000$, (c) $q = 5000$.

the other problem parameters remain unchanged. Figure 4 shows the "exact" solution and three finite-element solutions as a function of the angle θ, at $r = R$ and $t = 0.12$. The three finite-element solutions are those obtained by using on $\mathcal{B}$ the Sommerfeld condition; the DtN condition with only the zeroth term, i.e., $N = 0$; and the DtN condition with $N = 6$. It is clear that while the Sommerfeld solution and the $N = 0$ solution are rather poor, the $N = 6$ solution agrees well with the "exact" solution. Similar behavior is observed in Fig. 5, where these solutions are compared as functions of time at $r = R$ and $\theta = 0$.

We define the relative error $E = \|u^h - u_{ex}\|/\|u_{ex}\|$, where $\|\cdot\|$ is the $L_2(\mathcal{B})$ norm. In Fig. 6 we show this error (on a logarithmic scale) as a function of time, for four finite element solutions: the Sommerfeld solution and the DtN solutions with $N = 0$, $N = 2$, and $N = 6$. Note that the accuracy of the $N = 2$ and $N = 6$ solutions is much higher than that of the other solutions. The reason that the $N = 2$ solution is already quite accurate is that the second mode is the principal mode in the problem, as dictated by the boundary condition given on Γ. The small differences between the $N = 2$ and $N = 6$ solutions are due to the mode coupling that exists in this nonlinear problem.

For $f(u) = qu^2$ with the same boundary condition on Γ, we have obtained results which are similar in character to those shown previously in the axisymmetric case. The finite-element solution obtained by the procedure proposed here exhibits an unlimited growth, as predicted by theory, while the Sommerfeld-like boundary condition on $\mathcal{B}$ yields solutions which remain bounded.

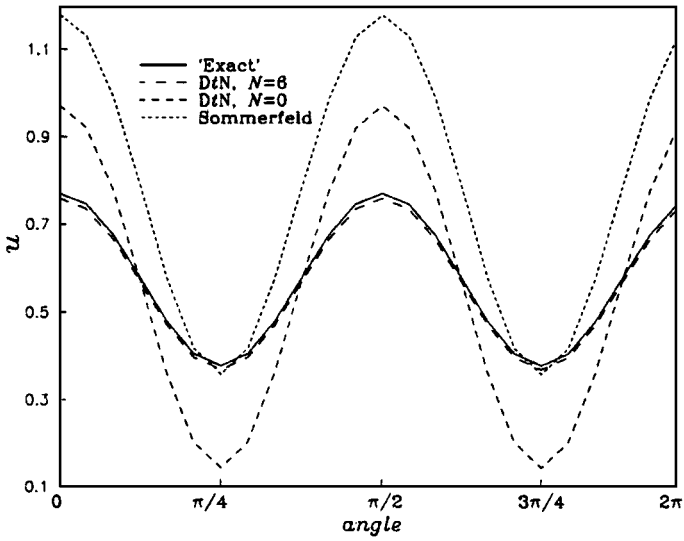

FIG. 4. An angle-dependent example, $f(u) = -qu^3$. Comparison of solutions as a function of the angle θ at $r = R$ and $t = 0.12$.

Finally, we solve a problem in which a "disturbance" propagates into the exterior domain across $\mathcal{B}$. We consider the same geometry as before, with $c = 17.5$, $f(u) = -qu^3$, and $q = 2 \times 10^4$. On the obstacle boundary Γ we prescribe $u = 0$ at time $t \geq 0$. We use a finite element mesh in Ω ($a \leq r \leq R$) which is much finer than the previous mesh, so as to resolve the propagation of a small disturbance. This disturbance is triggered through the *initial* condition. At time $t = 0$ we prescribe $u = 1$ at six nodes (all the other nodal values being zero): the nodes located at (0.333, 0) and (0.338, 0) and the four neighboring nodes located symmetrically with respect to the line $y = \theta = 0$. Figure 7 shows the solution along

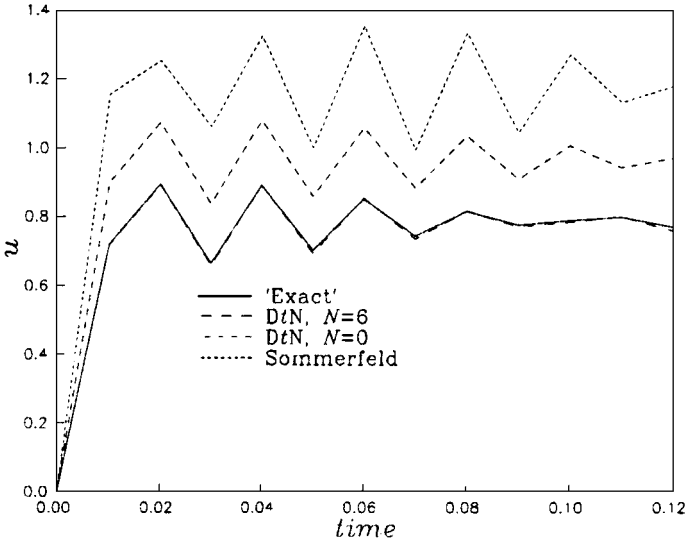

FIG. 5. An angle-dependent example, $f(u) = -qu^3$. Comparison of solutions as a function of time at $r = R$ and $\theta = 0$.

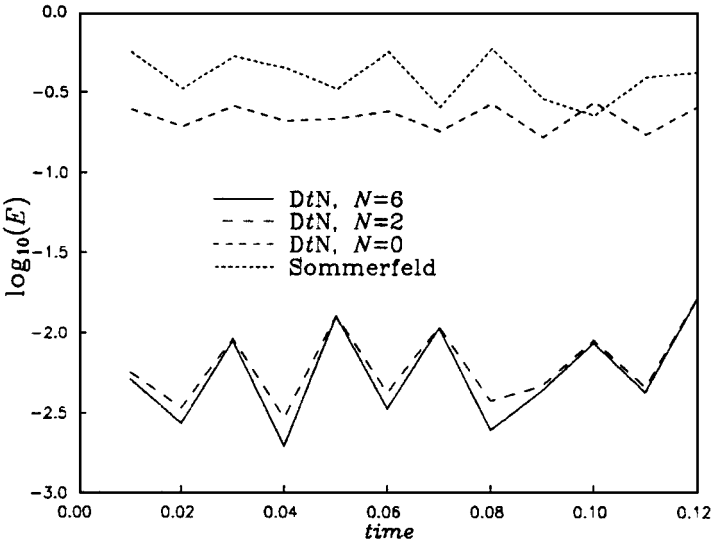

FIG. 6. An angle-dependent example, $f(u) = -qu^3$. Comparison of relative $L_2(\mathcal{B})$ errors as a function of time.

this radial line at different times. Note that while $\mathcal{B}$ is located at $r = R = 0.5$, the range of r values in the figure extends to $r = 2$. The direct wave and the wave reflected back from the obstacle at $r = a$ pass through $\mathcal{B}$ and propagate into the exterior domain. Clearly, some interesting coupling effects occur due to the wave nonlinearity.

9. CONCLUSION

In this paper we have proposed a finite-element scheme for the solution of nonlinear time-dependent exterior wave problems. In particular, we have concentrated on the two-dimensional nonlinear scalar (Klein–Gordon) equation as a relatively simple model in this category. The scheme is based on the Dirichlet-to-Neumann method which was originally developed for linear elliptic problems [6, 8–10]. In the DtN method the infinite domain is treated in an exact manner, thereby providing an accurate representation of the far field. Here the DtN method has been extended to the nonlinear time-dependent case. The new method draws from ideas used in [26] for the linear time-dependent case, and in [27] for the nonlinear elliptic equation $\nabla^2 u + f(u) = 0$. Additional relevant analysis can be found in [17, 30]. In the present context, we use the DtN boundary condition (44) which is exact for the time-discrete problem that is locally "linearized" via the simple iteration process.

In Ref. [27], other ways to linearize the problem in the exterior are considered (in the context of elliptic problems). One of them is based on treating the nonlinearity in an implicit way, which avoids the need for an internal fixed-point procedure at each time step. However, we show in [27] that the latter scheme is almost equivalent to the one proposed here in terms of the actual computation.

One ingredient of the proposed numerical method is an *implicit* time integration scheme. In this paper we have used the two-parameter Newmark family of time integrators (with $\beta > 0$), although any other implicit scheme can be used as well. Unfortunately, we have not yet found a way to extend the method such that *explicit* time integration schemes may be used with it.

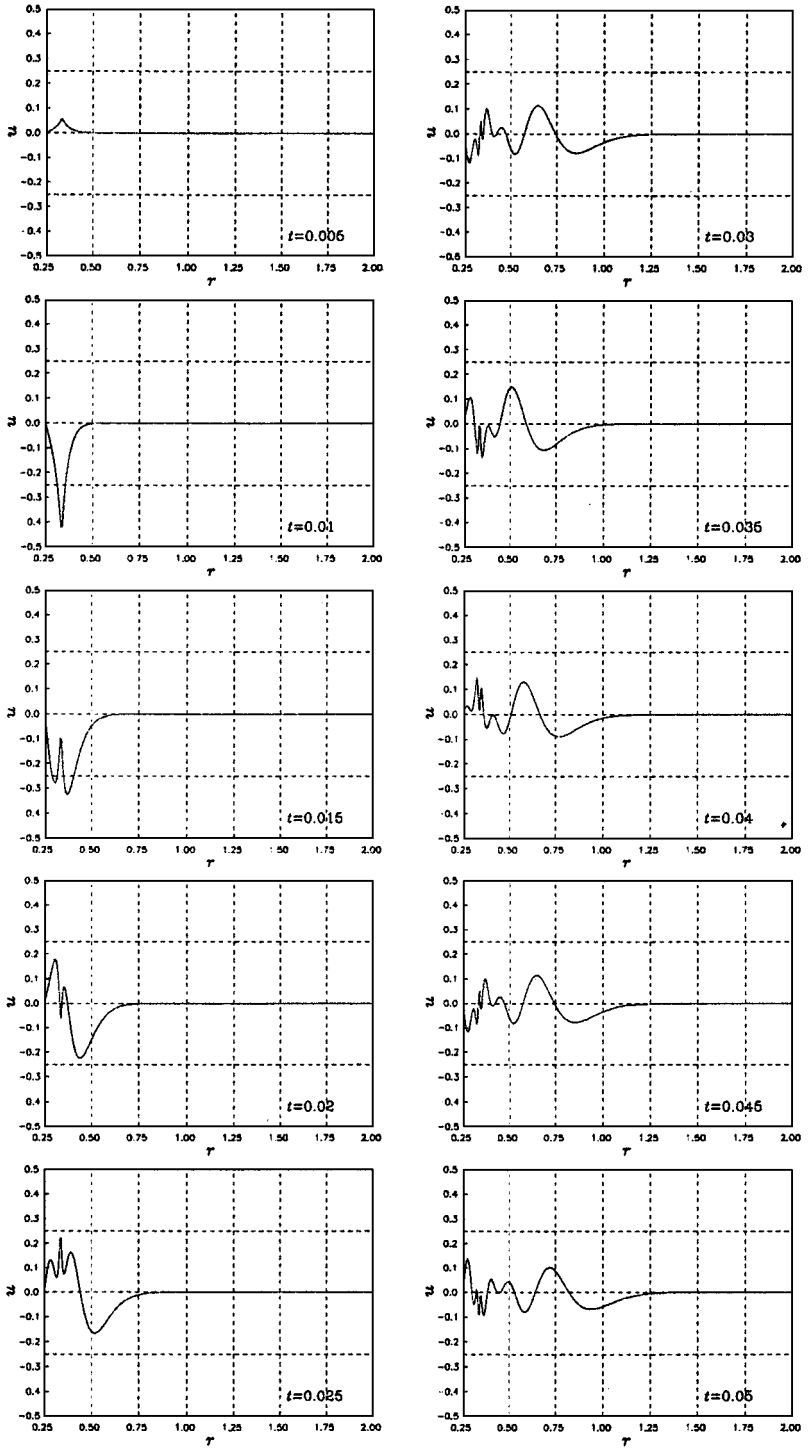

FIG. 7. Propagation of a small disturbance, $f(u) = -qu^3$. Solution along the radial line $y = \theta = 0$ at different times.

We have seen that a "naive" boundary condition on $\mathcal{B}$ like the Sommerfeld-like condition not only yields poor accuracy, but may alter the qualitative behavior of the numerical solution. In particular, when applied to problems whose exact solutions blow up in a finite time, the Sommerfeld-like condition produces bounded solutions. On the other hand, the DtN procedure proposed here captures the correct behavior of the solution.

The computational effort involved in the solution of nonlinear time-dependent wave problems in infinite domains is always quite large, and the present scheme is no exception. There is the inevitable tradeoff between accuracy and computational cost. For example, our method, in the way it is currently implemented, takes more CPU time (although much less memory!) than the simple scheme of using the Sommerfeld condition on a remote boundary $r = r_{\max}$. However, the implementation of our method may be made more efficient by (a) calculating and tabulating, as a preprocess, all the quantities that do not change with time, which depend only on a small number of parameters, so that they can be used repeatedly and efficiently during future computations; (b) using a small variable $r_{\max}$, as explained in Remark 3 of Section 7; (c) calculating the Fourier coefficients $\tilde{f}^c_m(\xi)$ and $\tilde{f}^s_m(\xi)$ in (41) by using FFT; (d) using more effective numerical integration schemes in the exterior (rather than the trapezoidal rule that we employ); and (e) replacing the fixed-point procedure by a more efficient scheme, along the lines of [27].

The nonlinear wave equation (1) has a deceivingly simple form, but the exterior problem already necessitates a quite complicated numerical scheme. Real challenges lie in the solution of yet more complex nonlinear exterior wave problems, such as problems of large-amplitude water waves and nonlinear elastic waves. We shall try to adapt the method devised here to these applications.

ACKNOWLEDGMENTS

This work was partly supported by the U.S.–Israel Binational Science Foundation (BSF), Grant 92-00016, and by the Fund for the Promotion of Research at the Technion. The first author thanks J. B. Keller, R. C. MacCamy, and J. Rubinstein for helpful discussions.

REFERENCES

1. G. B. Whitham, *Linear and Nonlinear Waves*, Wiley, New York, 1974.
2. T. W. Wright, ed., *Nonlinear Wave Propagation in Mechanics*, ASME Publications, New York, 1986.
3. L. A. Segel, *Mathematics Applied to Continuum Mechanics*, Dover, New York, 1987.
4. D. Givoli, *Numerical Methods for Problems in Infinite Domains*, Elsevier, Amsterdam, 1992.
5. A. A. Becker, *The Boundary Element Method in Engineering*, McGraw–Hill, London, 1992.
6. D. Givoli and J. B. Keller, A finite element method for large domains, *Comput. Meth. Appl. Mech. Eng.* **76**, 41 (1989).
7. D. S. Burnett, A three-dimensional acoustic infinite element based on a prolate spheroidal multipole expansion, *J. Acoust. Soc. Am.* **96**, 2798 (1994).
8. J. B. Keller and D. Givoli, Exact non-reflecting boundary conditions, *J. Comput. Phys.* **82**, 172 (1989).
9. D. Givoli and J. B. Keller, Non-reflecting boundary conditions for elastic waves, *Wave Motion* **12**, 261 (1990).
10. D. Givoli and S. Vigdergauz, Artificial boundary conditions for 2D problems in geophysics, *Comput. Meth. Appl. Mech. Eng.* **110**, 87 (1993).
11. D. Givoli, Non-reflecting boundary conditions, *J. Comput. Phys.* **94**, 1 (1991).
12. I. Harari and T. J. R. Hughes, Galerkin/least-squares finite element methods for the reduced wave equation with non-reflecting boundary conditions in unbounded domains, *Comput. Meth. Appl. Mech. Eng.* **98**, 411 (1992).

13. I. Harari and T. J. R. Hughes, Analysis of continuous formulations underlying the computation of time-harmonic acoustics in exterior domains, *Comput. Meth. Appl. Mech. Eng*. **97**, 103 (1992).
14. M. J. Grote and J. B. Keller, On non-reflecting boundary conditions, *J. Comput. Phys*. **122**, 231 (1995).
15. M. Malhotra and P. M. Pinsky, A matrix-free interpretation of the non-local Dirichlet-to-Neumann radiation boundary condition, *Int. J. Num. Meth. Eng*. **39**, 3705 (1996).
16. R. J. Astley, FE mode-matching schemes for the exterior Helmholtz problem and their relationship to the FE-DtN approach, *Commun. Num. Meth. Eng*. **12**, 257 (1996).
17. D. Givoli, I. Patlashenko, and J. B. Keller, High-order boundary conditions and finite elements for infinite domains, *Comput. Meth. Appl. Mech. Eng*. **143**, 13 (1997).
18. R. C. MacCamy and S. P. Marin, A finite element method for exterior interface problems, *Int. J. Math. Math. Sci*. **3**, 311 (1980).
19. C. I. Goldstein, A finite element method for solving Helmholtz type equations in wave guides and other unbounded domains, *Math. Comp*. **39**, 309 (1982).
20. C. Canuto, S. I. Hariharan, and L. Lustman, Spectral methods for exterior elliptic problems, *Numer. Math*. **46**, 505 (1985).
21. M. Masmondi, Numerical solution of exterior problems, *Numer. Math*. **51**, **87**, 101 (1987).
22. G. N. Gatica and G. C. Hsiao, The coupling of boundary integral and finite element methods for nonmonotone nonlinear problems, *Numer. Funct. Anal. Optim*. **13**, 431 (1992).
23. T. Hagstrom and H. B. Keller, Asymptotic boundary conditions and numerical methods for nonlinear elliptic problems on unbounded domains, *Math. Comput*. **48**, 449 (1987).
24. D. Givoli and D. Cohen, Non-reflecting boundary conditions based on Kirchhoff-type formulae, *J. Comput. Phys*. **117**, 102 (1995).
25. M. J. Grote and J. B. Keller, Exact non-reflecting boundary conditions for the time dependent wave equation, *SIAM J. Appl. Math*. **55**, 280 (1995).
26. D. Givoli, A spatially exact non-reflecting boundary condition for time dependent problems, *Comput. Meth. Appl. Mech. Eng*. **95**, 97 (1992).
27. D. Givoli and I. Patlashenko, Finite element schemes for nonlinear problems in infinite domains, *Int. J. Numer. Meth. Eng.*, to appear.
28. W. A. Strauss, *Nonlinear Wave Equations*, American Mathematical Society, Providence, RI, 1989.
29. R. Courant and D. Hilbert, *Methods of Mathematical Physics*, Vol. II, Wiley, New York, 1962.
30. I. Patlashenko and D. Givoli, A numerical method for problems in infinite strips with irregularities extending to infinity, *Num. Meth. Partial Differential Equations*, to appear.